

Supplementary Information for

Neutrophils promote tumor resistance to radiation therapy

Authors: Amy J. Wisdom, Cierra S. Hong, Alexander J. Lin, Yu Xiang, Daniel E. Cooper, Jin Zhang, Eric S. Xu, Hsuan-Cheng Kuo, Yvonne M. Mowery, David J. Carpenter, Kushal T. Kadakia, Jonathon E. Himes, Lixia Luo, Yan Ma, Nerissa Williams, Diana M. Cardona, Malay Halder, Yarui Diao, Stephanie Markovina, Julie K. Schwarz, and David G. Kirsch*.

*Corresponding Author: David G. Kirsch
Email: david.kirsch@duke.edu

This PDF file includes:

- Supplementary materials and methods
- Figs. S1 to S13
- Tables S1 to S8
- References for SI reference citations

Supplementary Materials and Methods

Cervical cancer clinical data

TCGA Data Analysis

The most updated clinical data for the TCGA cervical cancer cohort (accessed December 19th, 2018), including patient outcome and status of radiation therapy, were extracted using TCGAAbiolinks (1) from NCI Genomic Data Commons (2). One hundred sixty-nine TCGA cervical cancer patients completed radiation therapy and were included for the Kaplan-Meier analysis of overall survival after radiation therapy. Relative fractions of neutrophils in primary tumors for the TCGA cervical cancer cohort were extracted from Supplementary Table 1 of the TCGA consortium study on the immune landscape of cancer (3). The relative fractions of neutrophils were estimated using CIBERSORT (4) and normalized by the leukocyte fraction for each sample.

Cervical cancer patients from Washington University in St. Louis

Cervical cancer patients who completed curative-intent radiation at a single academic institution (Washington University in St. Louis) from 2006-2017 were retrospectively reviewed with approval of the institutional review board with a waiver of consent (protocol # 201807063). Patients with at least one complete blood count (CBC) during radiation to 6 months post-radiation were included. Patients with FIGO stage IA1/2 or IVB, evidence of distant metastasis on imaging, and rare histologies were excluded. All patients were staged with physical exam and lymph node involvement was determined by ^{18}F -fluorodeoxyglucose positron emission tomography (^{18}F FDG-PET). The treatment approach including external beam radiation and weekly intracavitary brachytherapy in this cohort, as well as follow up, has been previously described (5). 90% of patients received platinum-based chemotherapy concurrently with radiation. Absolute neutrophil count (ANC), absolute lymphocyte count (ALC), hemoglobin concentration, and platelet count were obtained as a part of routine clinical care, and were entered into univariable Cox regression for any cervical cancer recurrence at pre-radiation, week 1 of radiation, week 3 of radiation, week 6-8 of radiation, and 12-26 weeks post-radiation start time points. Significant clinical variables were modeled with multivariable Cox regression in a backward-

conditional manner. Cumulative hazard and Kaplan-Meier plots were used to show estimated rates of cervix recurrence, pelvic recurrence, distant recurrence, and cause specific survival. Significance was set at $p < 0.05$ and all statistical tests were two-sided. Statistics were done in SPSS, version 23 (IBM, Armonk, NY).

Experimental design

The goal of these controlled laboratory experiments was to determine the role of neutrophils in the response to radiation therapy. We used genetically engineered mice and observed histological and growth delay endpoints. Based on published autochthonous sarcoma radiation response data from the laboratory and power calculations performed as described previously (6), sample sizes were selected before initiating the study. Outliers were defined as falling greater than 2 standard deviations from the mean. No outliers were excluded from this study. The mice in this study were randomized to their treatments. Investigators were not blinded when performing sarcoma measurements. Histological and flow cytometric quantification were performed by an observer blinded to treatment and genotype. Histological assessment of sarcomas with and without genetic neutrophil depletion was performed by a sarcoma pathologist (D.M.C.) who was blinded to treatment and genotype.

Mouse strains and tumor induction

All animal studies were performed in accordance with protocols approved by the Duke University Institutional Animal Care and Use Committee (IACUC) and adhere to the NIH Guide for the Care and Use of Laboratory Animals. All alleles used in this study have been described previously, including *Kras*^{LSL-G12D/+} (7), *Trp53*^{flox/flox} (7), *Kras*^{FSF-G12D/+} (8), *Trp53*^{FRT/FRT} (8), *MRP8*^{Cre} (9), *R26*^{LSL-tdTomato/+} (10), and *R26*^{LSL-DTX/+} (11). Primary soft tissue sarcomas were generated with intramuscular (IM) injection of an adenovirus expressing either Cre recombinase (Adeno-Cre; Viral Vector Core, Iowa City, IA) or Flippase recombinase (Adeno-FlpO; Viral Vector Core, Iowa City, IA) in mice that were 5-10 weeks of age. Twenty-five μL of adenovirus was mixed with 600 μL DMEM 1X (Gibco, ref 11995-065) and 3 μL 2M CaCl_2 , then incubated for 15 minutes prior to injection. Fifty μL of the prepared mixture was injected into the gastrocnemius muscle of the mice. *Kras*^{LSL-G12D/+}; *Trp53*^{flox/flox} mice were maintained on a pure 129/SvJae genetic background and all other mice were on a

mixed genetic background. To minimize the effects of genetic background, age-matched littermate controls were used for every experiment so that potential genetic modifiers would be randomly distributed between experimental and control groups.

Tumor treatment and measurement

When the tumors reached 70-150 mm³, the sarcomas were randomized and treated with a small animal micro-irradiator (12) and monitored three times weekly by caliper measurement in two dimensions. Sarcoma irradiations were performed using the Precision Xrad 225Cx small animal image-guided irradiator. The irradiation field was centered on the target via fluoroscopy with 40 kilovolt peak (kVp), 2.5 mA x-rays using a 2 mm aluminum filter and a 0.3 mm copper filter. Sarcomas were irradiated with parallel-opposed anterior and posterior fields with an average dose rate of 300 cGy/min prescribed to midplane with 225 kVp, 13 mA x-rays using a 0.3-mm copper filter and a collimator with a 40 × 40 mm² radiation field at treatment isocenter. Anti-Ly6G antibody depletion (BioXCell BP0075-1, clone 1A8, 200 μL/treatment at 1 mg/mL diluted in PBS, injected intraperitoneally) was initiated when sarcomas reached 70-150 mm³ (Day 0) and repeated on Days 3, 6, 9, and 12. Twenty-four hours after the start of antibody treatment (Day 1), mice received focal irradiation with 20 Gy to the site of the tumor. The same methods were used for treatment with anti-CD3 antibody (BioXCell BE0002, clone 17A2) or isotype control (BioXCell BE0090, Clone LTF-2). After treatment initiation, tumors were measured three times per week for growth delay. Tumor volumes were calculated using the following formula: $\pi/6 (\text{smaller dimension})^2 \times (\text{larger dimension})$. Relative tumor volumes were calculated as the tumor volume at a given time point divided by the tumor volume at the time of treatment start. Mice were euthanized if moribund or when tumor volumes reached more than 13 mm³ in any dimension in accordance with IACUC guidelines at Duke University. For tissues harvested 48 hours after radiation therapy for pimonidazole staining (Fig. S13), mice were euthanized by cervical dislocation. All other mice were euthanized with CO₂.

Murine bone marrow transplant

Whole bone marrow (WBM) cells were isolated from femurs and tibias of healthy mice on a 129/SvJae genetic background by washing the bone marrow space with phosphate buffer saline (PBS; pH 7.4, Gibco). Red blood cells (RBCs) were lysed using ACK lysing buffer (Lonza). Total number of WBM cells was counted with a cellometer cell counter (Cellometer Auto 2000, Nexcelom Bioscience) and AO/PI stain (cat CS2-0106-5ML, Nexcelom Bioscience). Three million WBM cells were resuspended in 50 μ L PBS and injected retro-orbitally into recipient mice.

Primary sarcoma dissociation and staining for flow cytometric analysis

Tumors were dissected and minced before dissociation per manufacturer's instructions for tough murine tumors using MACS C tubes and the mouse Tumor Dissociation Kit (Miltenyi Biotec). After the tumor dissociation was completed, the cells were filtered through a 40 μ m strainer. RBCs were lysed using ACK Lysing Buffer (Lonza) and washed with flow buffer made of HBSS (cat 13175-095, Gibco), 5 mM EDTA (E7889, Sigma-Aldrich), and 2.5% fetal bovine serum (FBS; Gibco). The cells were blocked with purified rat anti-mouse CD16/CD32 (BD Pharmingen, dilution 1:100) then stained with the appropriate flow antibodies for 25 minutes on ice. After washing, the cells were fixed in 1% paraformaldehyde (PFA; ThermoFisher Scientific). Relevant antibodies and compensation beads used for flow cytometry analysis are in Table S8. Flow cytometry was performed in the Duke Human Vaccine Institute Flow Cytometry Facility (Durham, NC) using the BD LSR II cytometer. For FACS and Wright staining, dissociation, RBC lysis, and blocking were performed as described above. Whole tumor cells were stained with Live/Dead Zombie Aqua (Biolegend, 1:500) for 15 minutes and viable tdTomato⁺ cells were collected. Cells were then mounted, dried for 2 hrs, and Wright stained.

Immunohistochemistry

Fresh tumor samples were harvested after euthanasia, fixed in 4% PFA overnight, and preserved in 70% ethanol until paraffin embedding. For tumor samples harvested 48 hours after treatment for hypoxia staining, mice were injected intraperitoneally with pimonidazole (Hypoxyprobe, HP-100mg) 1hr before euthanasia. For NG2 and pimonidazole staining, immunohistochemistry was performed with the ABC kit (Vector Laboratories, PK-7200)

using antibodies to NG2 (Sigma, AB5320, 1:250) and pimonidazole (Hypoxyprobe, Pab2627, 1:250). Sections were developed with 3,30 -diaminobenzidine and counterstained with haematoxylin (Sigma-Aldrich, H3136). To stain for CD31, the immunohistochemistry protocol for paraffin-embedded tissues from Cell Signaling Technologies was followed. Briefly, five-micron sections were deparaffinized with xylene and rehydrated with ethanol and water washes. They were incubated in 1X Citrate Unmasking Solution (Cell Signaling, 14746S) at 98°C for 10 minutes, then allowed to cool for 30 minutes. Sections were incubated with 3% hydrogen peroxide for 10 minutes, washed, then blocked for 1 hour at room temperature in 5% normal goat serum (VECTOR) diluted in 0.3% Tween 20 PBS solution (PBST). After washing, tissues were incubated overnight in anti-CD31 primary antibody (Cell Signaling, 77699, 1:100) diluted in 5% normal goat serum and SignalStain Antibody Diluent (Cell Signaling, 8112L). The following day, tissues were washed in PBS and incubated with SignalStain Boost Detection Reagent (Cell Signaling, 8114) for 30 minutes. Tissues were then stained with SignalStain DAB Substrate Kit (Cell Signaling, 8059) for 2 minutes, washed in water, and counterstained with Mayer's hematoxylin solution (Sigma-Aldrich) for 1 minute. Tissue sections were washed in water and dehydrated prior to mounting samples with coverslips using permanent mounting medium (Leica Micromount, 3801732). Three representative images of each section were obtained with a Leica DM 2000 LED microscope at 40x magnification. Using ImageJ (National Institutes of Health), positive staining was quantified manually and averaged per tumor section.

Mouse peripheral complete blood count

At indicated time points, 100 µL circulating blood was drawn from the submandibular vein and the Duke University Division of Laboratory Animal Resources (DLAR) performed complete blood count analysis using the ProCyte Dx analyzer (IDEXX Laboratories, Inc.).

Fine needle aspiration of primary sarcomas and staining for flow cytometry

A BD Luer Lock Syringe (Air-Tite Products Co., Inc.) and 22.5-gauge needle (Air-Tite Products Co., Inc.) were used to aspirate cells from the tumor. RBCs were lysed for 2 minutes with ACK Lysing Buffer (Thermo

Scientific) and washed with a solution buffer of HBSS, 5mM EDTA (E7889, Sigma-Aldrich), and 2.5% FBS (Gibco). The cells were then stained with the appropriate flow antibodies and fixed in 1% PFA.

Single-cell RNA sequencing

Tumors were dissected and minced before dissociation per manufacturer's instructions for tough murine tumors using MACS C tubes and the mouse Tumor Dissociation Kit (Miltenyi Biotec). After the tumor dissociation was completed, the cells were filtered through a 40 μ m strainer. RBCs were lysed using ACK Lysing Buffer (Lonza) and washed with flow buffer made of HBSS (cat 13175-095, Gibco), 5 mM EDTA (E7889, Sigma-Aldrich), and 2.5% fetal bovine serum (FBS; Gibco). Tumors were washed twice more in 0.04% BSA in PBS, then resuspended at 1000 cells per μ L. Cell suspensions were loaded on the 10x Genomics Chromium Controller Single-Cell Instrument (10x Genomics) using the Chromium Single Cell 3' Reagent V3 Kit. Cells were mixed with reverse transcription reagents, gel beads, and oil to generate single-cell gel beads in emulsions (GEM) for reverse transcription (RT). After RT, GEMs were broken and the single-stranded cDNA was purified with DynaBeads. cDNA was amplified by PCR and the cDNA product was purified with the SPRIselect Reagent Kit (Beckman Coulter). Sequencing libraries were constructed using the reagents provided in the Chromium Single-Cell 3' Library Kit following the user guide. Sequencing libraries were sequenced with the Illumina platform at Novogene.

Single-cell RNA sequencing data analysis

Raw gene expression matrices were generated using CellRanger (v3.0.1) and converted to the Seurat object using Seurat (v3.0.1) (13). The data were normalized on a log scale after filtering for minimal UMI and cell observance frequency according the Seurat documents (http://satijalab.org/seurat/pbmc3k_tutorial.html). Unwanted sources of variation, including the total cellular read count and mitochondrial reads, were removed using the regress method provided in the Seurat *ScaleData* function. Principal components were calculated using the most variably expressed genes and the first 10 principal components were carried forward for clustering and visualization. Cells were embedded into a K-nearest neighbor graph using the *FindNeighbors*

function and iteratively grouping cells together with the Louvain algorithm using the *FindClusters* function. The Uniform Manifold Approximation and Projection (UMAP) dimensionality reduction method was used to place similar cells together in two-dimensional space. Cluster biomarkers were identified using the *FindAllMarkers* function and visualized on the UMAP plot to show individual cell types. Differentially expressed genes between tumors treated with anti-Ly6G + 20 Gy and isotype + 20 Gy were identified using the Wilcoxon test (genes with fold change >1 and p value < 0.05 were defined as statistically significant). Gene set enrichment analysis was performed using the GSEA method in the fgsea R package (14) with pathway annotations from the Reactome Pathway Knowledgebase (15). Heat maps were generated using Complexheatmap (16). Single-cell RNA sequencing data are available at synapse.org (Synapse ID: syn18918968). The analysis of single-cell RNA sequencing used Extreme Science and Engineering Discovery Environment Stampede2 (17).

Fig. S1.

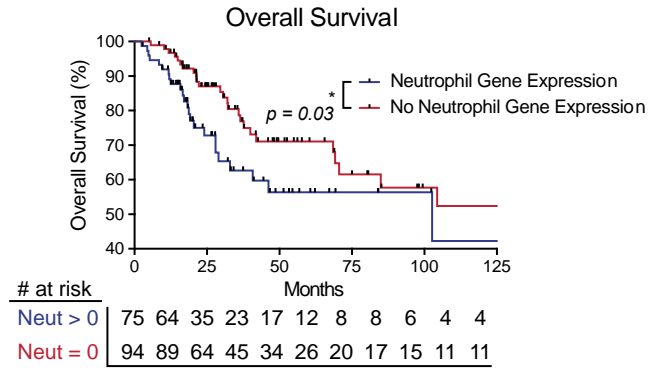


Fig. S1. Neutrophils correlate with poor outcomes after chemoradiotherapy in cervical cancer patients.

CIBERSORT analysis of TCGA-CESC data (n=169) for all cervical cancer patients who received radiation therapy with (blue) or without (red) neutrophil gene expression signature.

Fig. S2.

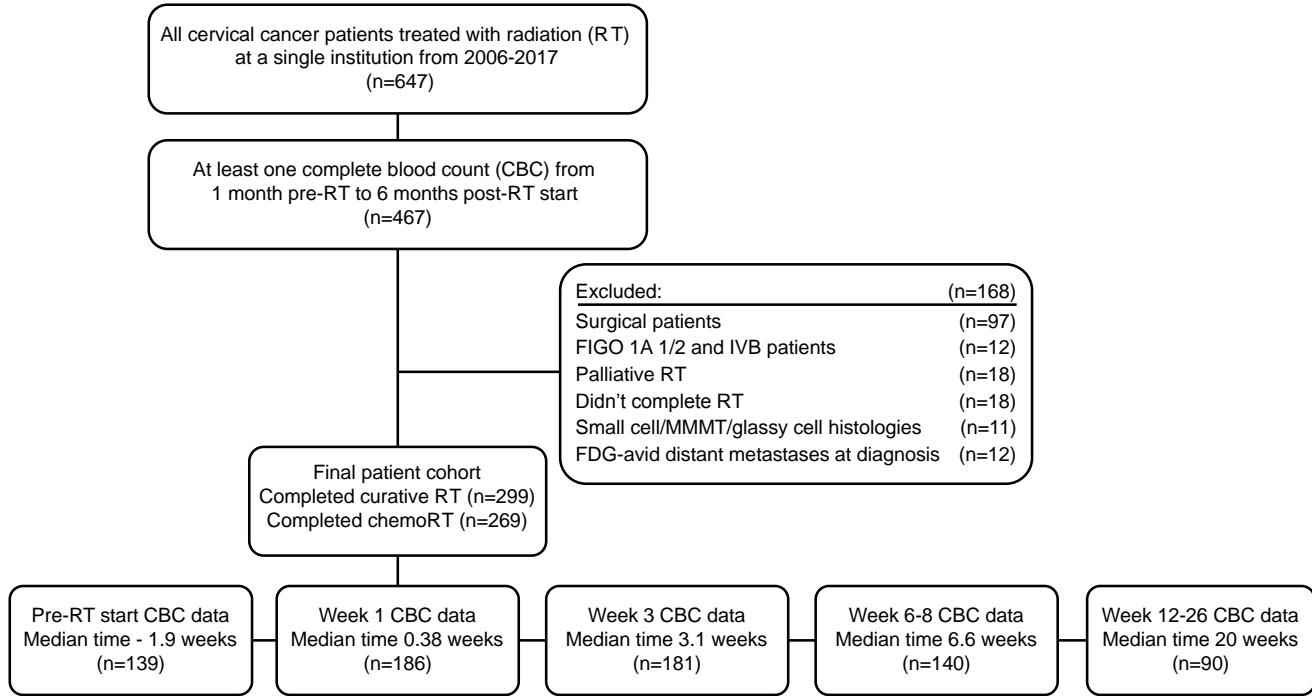


Fig. S2. CONSORT diagram for cervical cancer patients included in the study.

Fig. S3.

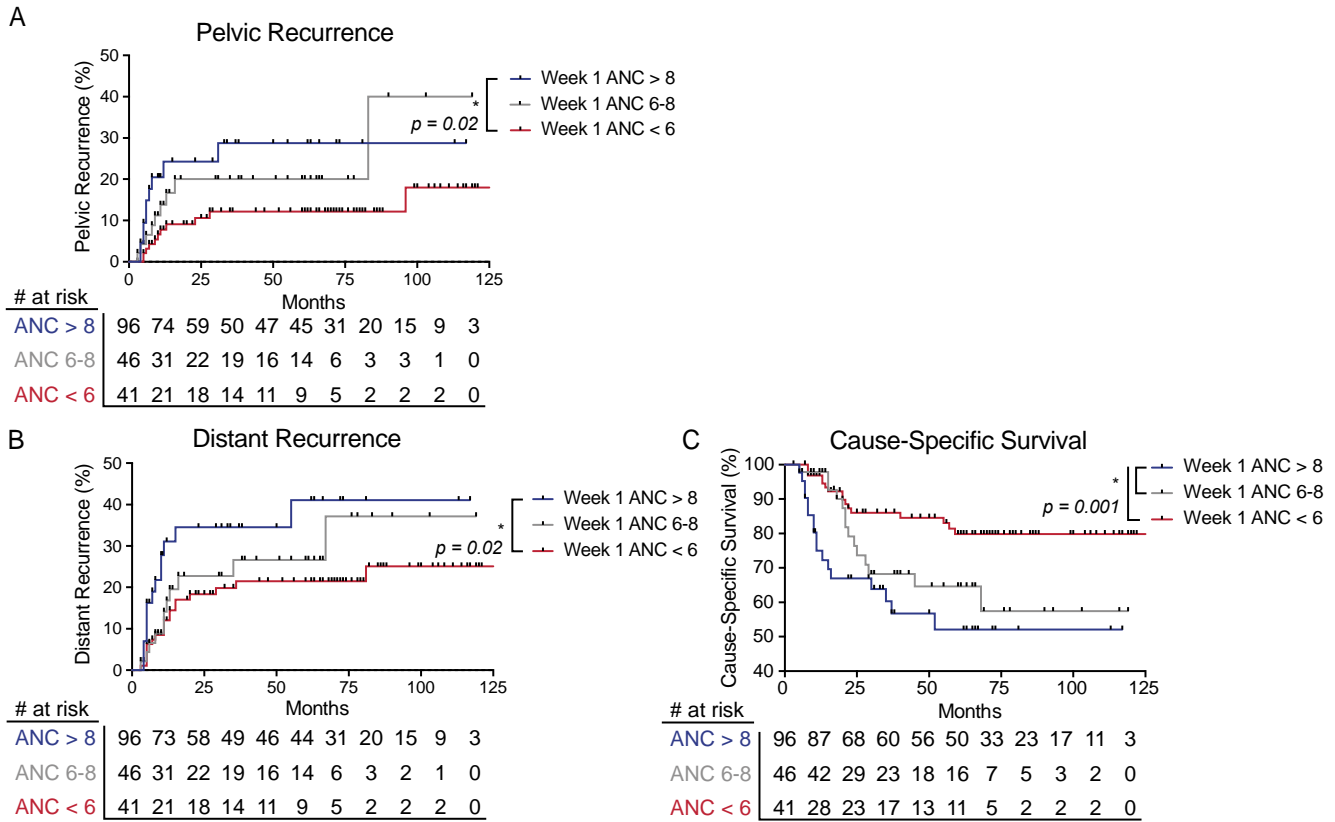


Fig. S3. Neutrophils correlate with poor outcomes after chemoradiotherapy in cervical cancer patients. **A-C)**

Association between week 1 ANC levels (ANC > 8: blue; ANC 6-8: gray; ANC < 6: red) and **A)** pelvic recurrence, **B)** distant recurrence, and **C)** cervical cancer cause-specific survival for patients treated with chemoradiotherapy. Data were calculated with the Kaplan-Meier method and analyzed by the log-rank test.

Fig. S4.

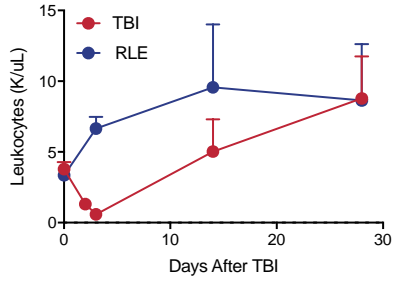


Fig. S4. Total body irradiation depletes leukocytes. Circulating leukocytes were measured at indicated time points by complete blood count from tumor-bearing mice after focal tumor irradiation (blue) or total body irradiation (TBI, red). Error bars represent mean \pm SEM. For focal group (blue) n=2 at D0, D3, D14, and D28. For TBI group n=3 at D0, n=3 at D2, n=2 at D3, n=5 at D14, and n=5 at D28.

Fig. S5.

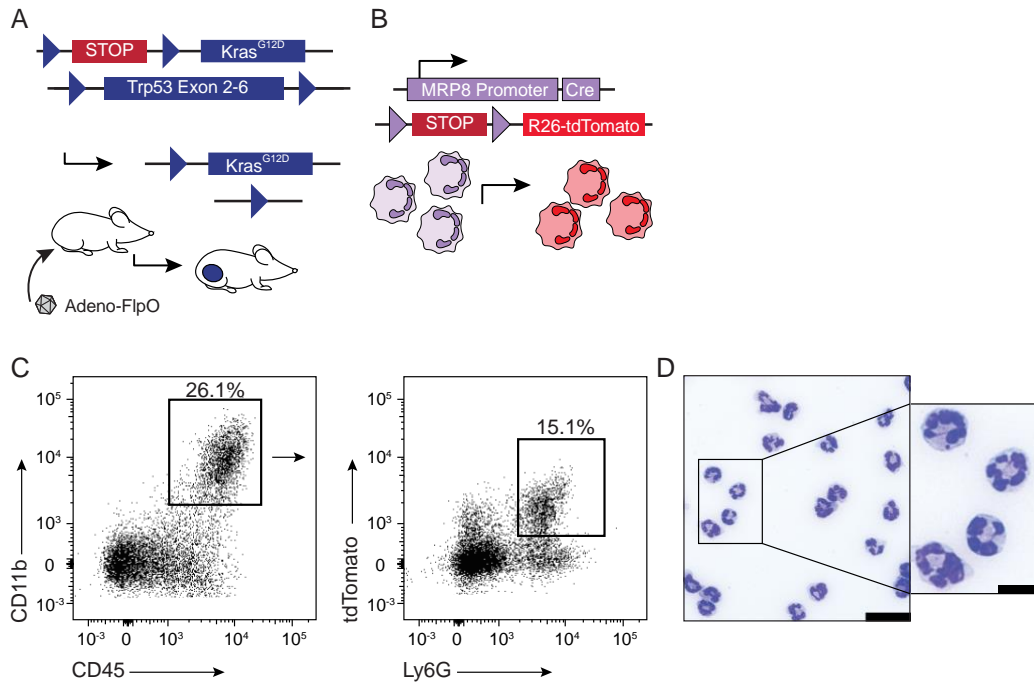


Fig. S5. Fluorescent labeling of tumor-infiltrating neutrophils. **A)** Genetic strategy to activate oncogenic *Kras*^{G12D} expression and delete *Trp53* alleles in tumor cells by FlpO-mediated recombination at FRT sites (blue arrows) and **B)** to activate expression of tdTomato in neutrophils by expression of Cre recombinase under the MRP8 promoter. **C)** Representative flow cytometry from the tumor of an unirradiated *FSF-Kras*^{G12D/+}; *Trp53*^{FRT/FRT}; *MRP8*^{Cre}, *R26*^{LSL-tdTomato/+} (KPMT) mouse. **D)** Live tdTomato⁺ cells were isolated by FACS from the tumor of an unirradiated KPMT mouse and Wright stained. Scale bars: 100 μm and 20 μm (inset).

Fig. S6.

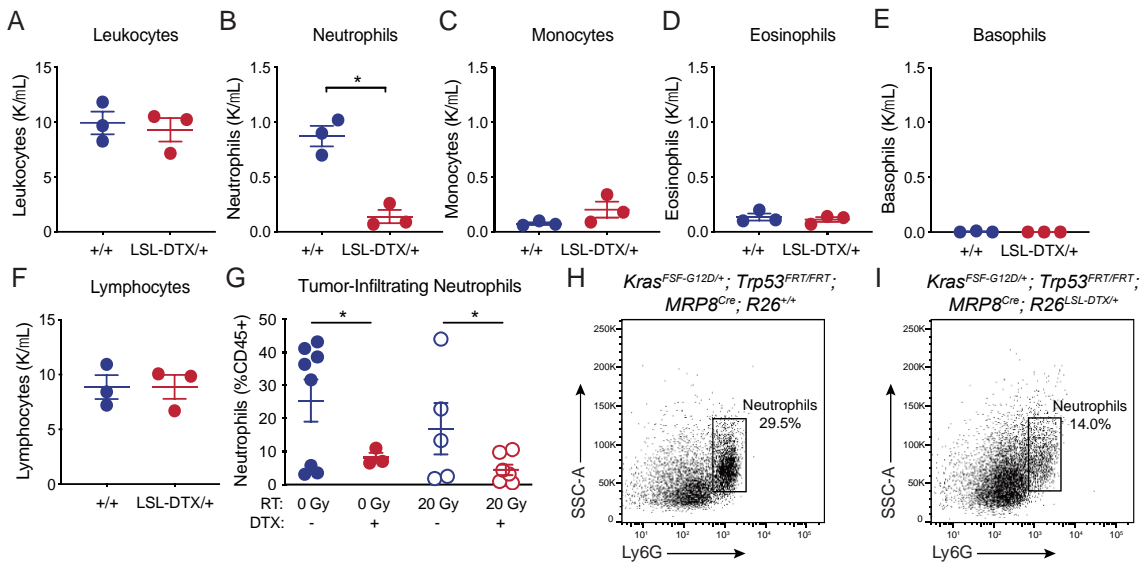


Fig. S6. MRP8-mediated genetic depletion of neutrophils. CBC drawn from 6-week old non-tumor bearing mice measuring **A)** leukocytes, **B)** neutrophils, **C)** monocytes **D)** eosinophils, **E)** basophils, and **F)** lymphocytes in mice with MRP8-driven expression of Cre and either wild type *Rosa26* (*R26*^{+/+}, blue) or Cre-activated expression of diphtheria toxin (*DTX*) at *Rosa26* (red, *R26*^{LSL-DTX/+}). **G)** Neutrophil (CD11b⁺ Ly6G⁺ SSC^{hi} of viable CD45⁺ cells) infiltration into sarcomas from mice with depleted (red) or intact (blue) neutrophils 7 days after either 0 Gy (filled circle) or 20 Gy (open circle) radiation. Error bars represent mean \pm SEM. **H)** Representative flow cytometry plot of tumor-infiltrating neutrophils in KPM mice with retained neutrophils or in KPMD mice with **I)** depleted neutrophils (gated on viable CD11b⁺ CD45⁺ cells).

Fig. S7.

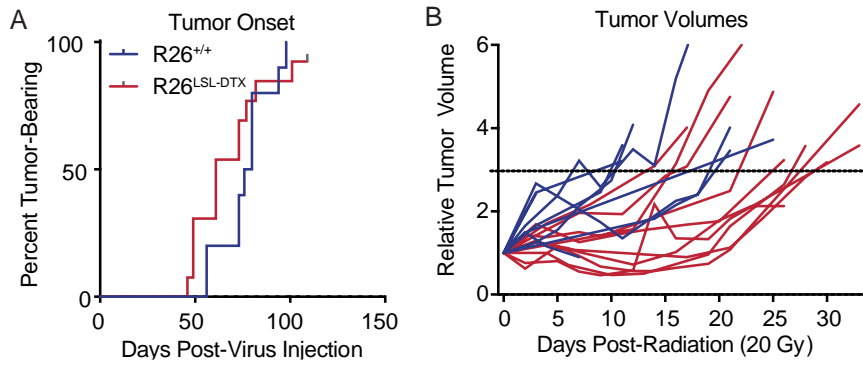


Fig. S7. Genetic depletion of neutrophils radiosensitizes soft tissue sarcomas. **A)** Time to tumor onset (defined as the day when tumor volume reaches 70-150 mm³) for sarcomas in KPM (blue) and KPMD (red) mice. **B)** Relative tumor volume (volume at each time point divided by volume at time of treatment) for irradiated tumors in KPM (blue) and KPMD (red) mice. Line at relative tumor volume of 3 (tumor tripling).

Fig. S8.

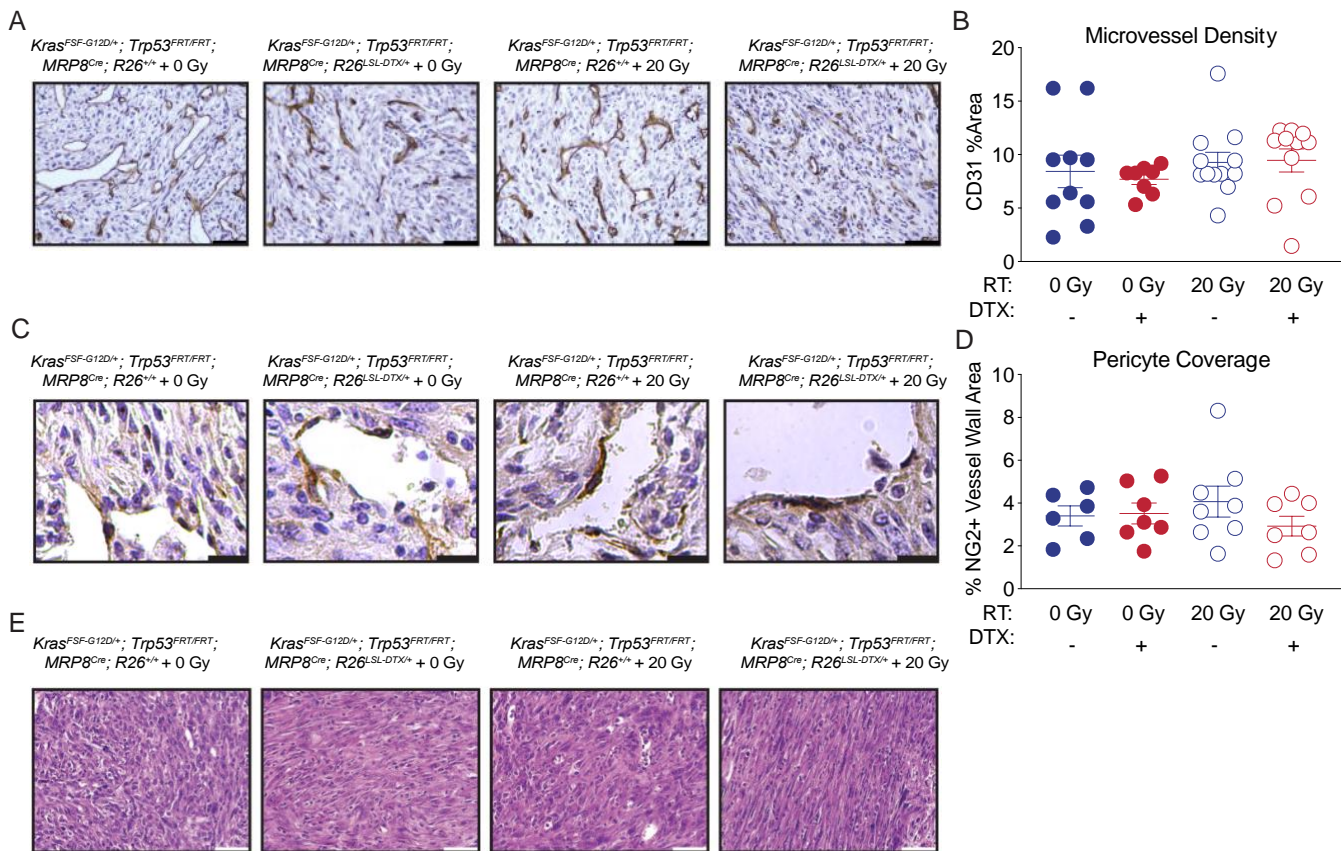


Fig. S8. Vessel density in sarcomas with genetic neutrophil depletion. **A**) Representative images and **B**) Quantification of CD31⁺ cells (% area) in sarcomas from KPM (blue) and KPMD (red) mice 7 days after 0 Gy (filled circles) or 20 Gy (open circles) radiation for mice with depleted (red) or intact (blue) neutrophils. **C**) Representative images and **D**) Quantification of NG2⁺ pericytes per vessel area in sarcomas from KPM (blue) and KPMD (red) mice 7 days after 0 Gy (filled circles) or 20 Gy (open circles) radiation. Error bars represent mean \pm SEM. **E**) Representative hematoxylin and eosin stained sections of primary sarcomas 7 days after treatment for tumors of indicated genotypes and treatments. Scale bars: 100 μ m in Panel A; 25 μ m in Panel C; 100 μ m in Panel E.

Fig. S9.

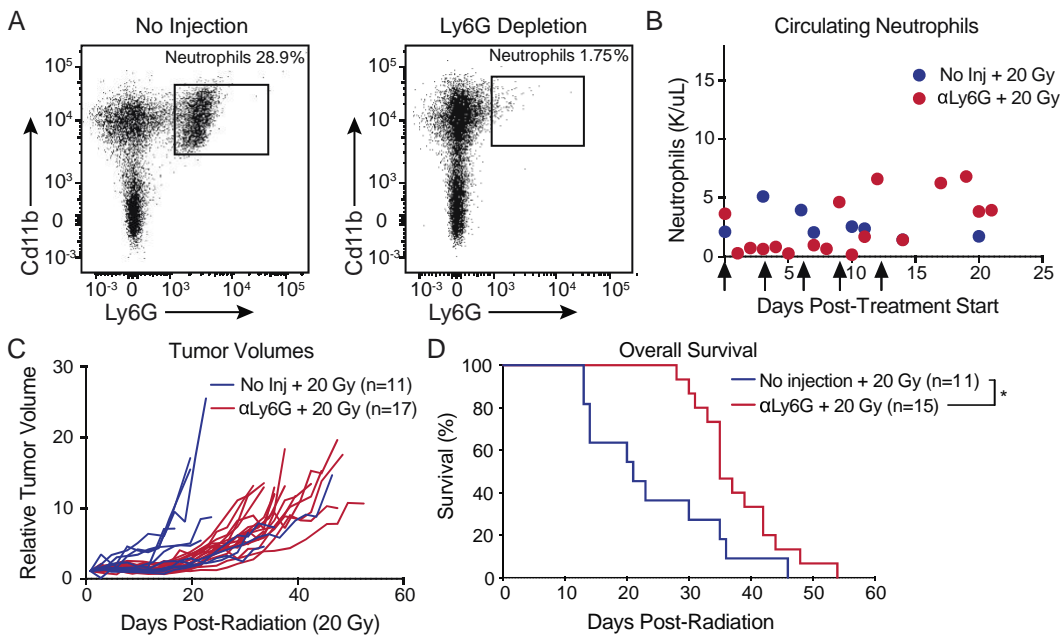


Fig. S9. Antibody-mediated depletion of neutrophils. **A)** Tumor-infiltrating neutrophils (CD11b⁺ Ly6G⁺) in sarcomas that received 20 Gy radiation therapy in mice three days after treatment with either no injection or anti-Ly6G depletion. **B)** Quantification of circulating neutrophils measured by complete blood count collected from a submandibular vein at 1, 4, 7, and 11 days after treatment start. Mice were treated with radiation and anti-Ly6G antibody (red) or without antibody (blue) when tumor size reached 70-150 mm³ (Day 0) and Days 3, 6, 9, and 12 (arrows). **C)** Relative tumor volume (volume at each time point divided by volume at start of treatment) for tumors in mice treated with 20 Gy and with (red) or without (blue) anti-Ly6G antibody. **D)** Kaplan-Meier plot of mouse survival in mice with depleted (red) or intact (blue) neutrophils after irradiation with 20 Gy (n = 15 and 11 mice per group, respectively). Log-rank test showed that the difference was statistically significant ($p = 0.002$).

Fig. S10.

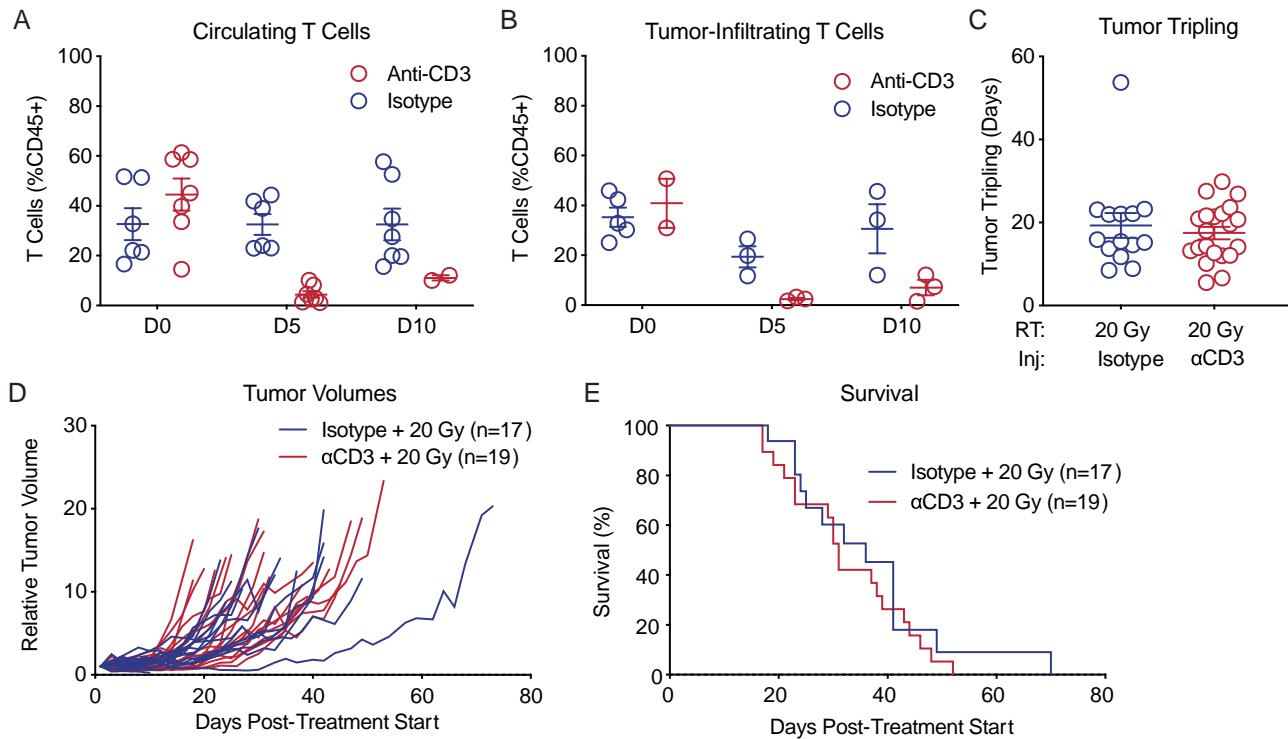


Fig. S10. Pharmacologic depletion of T cells does not radiosensitize soft tissue sarcomas. **A)** Circulating T cells in mice that received 20 Gy radiation therapy in mice three days after treatment with either isotype control antibody or anti-CD3 T cell depletion. **B)** Quantification of tumor-infiltrating T cells measured by flow cytometric analysis of cells serially collected from sarcomas by fine needle aspiration at 0, 5, or 10 days after treatment initiation. Mice were treated with anti-CD3 antibody (red) or isotype control antibody (blue) when tumor size reached 70-150 mm³ (Day 0) and Days 3, 6, 9, and 12. Error bars represent mean \pm SEM. **C)** Time to tumor volume tripling after treatment with 20 Gy and either anti-CD3 antibody (red) or isotype control (blue). Error bars represent mean \pm SEM. **D)** Relative tumor volume (volume at each time point divided by volume at start of treatment) for tumors in mice treated with 20 Gy and either anti-CD3 antibody (red) or isotype control (blue). **E)** Kaplan-Meier plot of mouse survival in mice with depleted (red) or intact (blue) T cells after irradiation with 20 Gy (n = 19 and 17 mice per group, respectively). Log-rank test showed that the difference was not statistically significant ($p = 0.4215$).

Fig. S11.

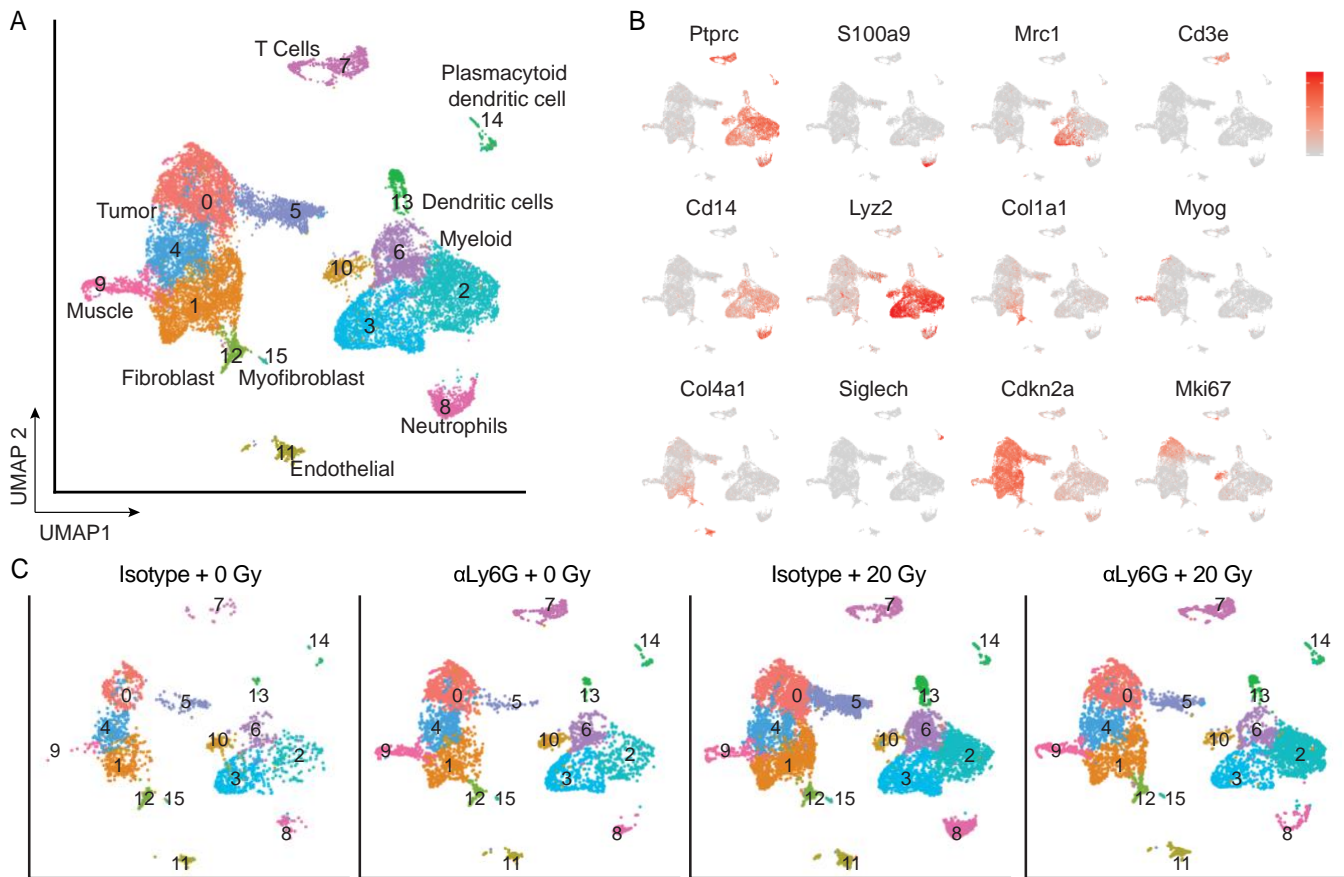


Fig. S11. Single-cell RNA sequencing of neutrophil-depleted and neutrophil-intact primary sarcomas treated with or without radiation therapy. **A)** UMAP plots of scRNA-seq data demonstrate all clusters from all samples. $n = 2$ mice per group; 19,056 single cells total (Isotype + 0 Gy $n = 1860$; anti-Ly6G + 0 Gy $n = 4024$; Isotype + 20 Gy $n = 7914$; anti-Ly6G + 20 Gy $n = 5258$). **B)** Relative expression levels of selected genes, normalized for sequencing depth. **C)** Distribution of cells, separated by treatment group.

Fig. S12.

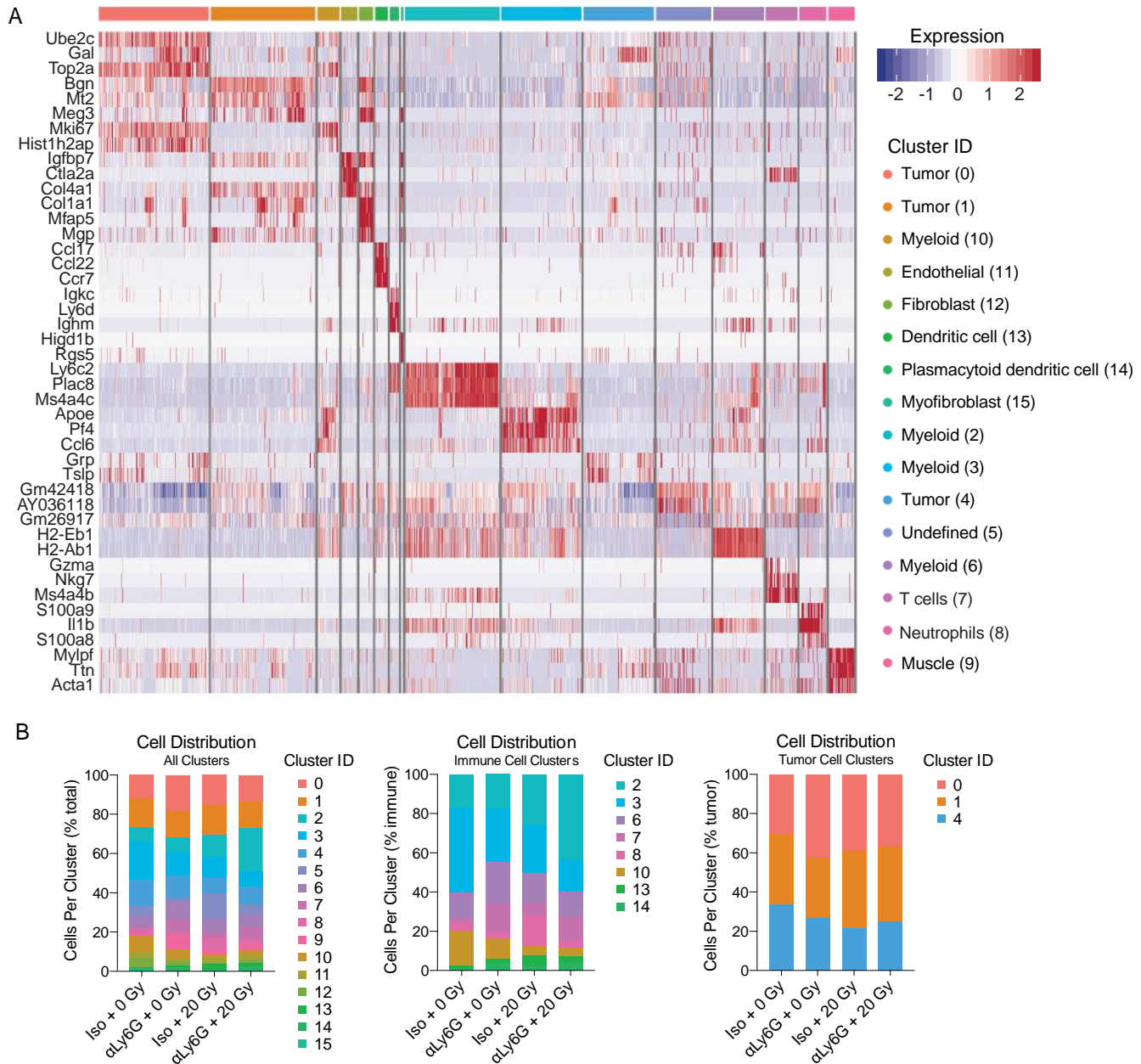


Fig. S12. Effects of neutrophil depletion and radiation therapy at single cell resolution. **A)** Heat map of top 3 marker genes expressed in each cluster. **B)** Frequency of cell distribution across all clusters, immune cell clusters, and tumor cell clusters for each treatment group.

Fig. S13.

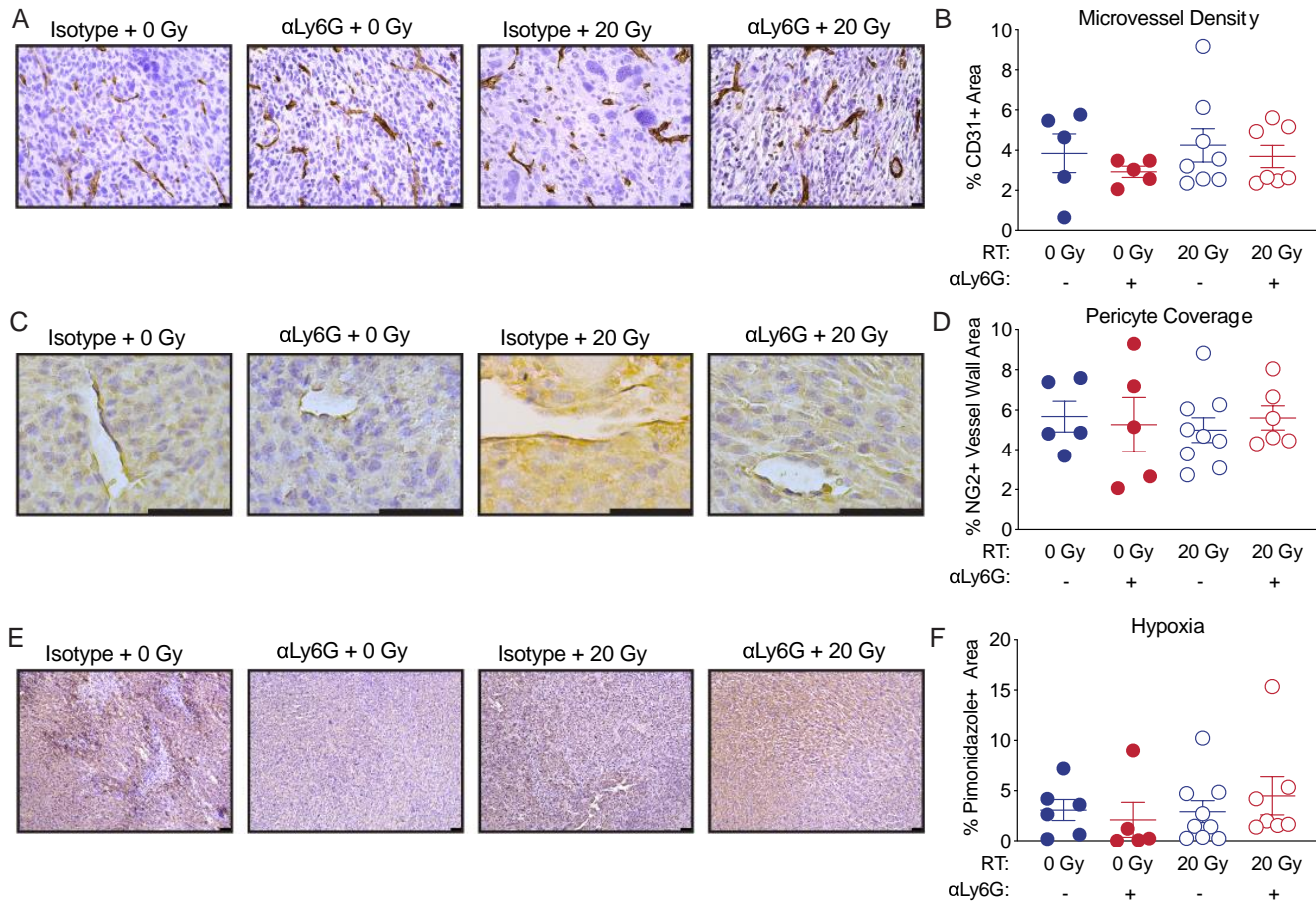


Fig. S13. Vessel density and hypoxia in sarcomas with antibody-mediated neutrophil depletion. **A**) Representative images and **B**) Quantification of CD31⁺ cells (% area) in sarcomas from mice treated with isotype control antibody (blue) or anti-Ly6G antibody (red) 48 hours after 0 Gy (filled circles) or 20 Gy (open circles) radiation. **C**) Representative images and **D**) Quantification of NG2⁺ pericytes per vessel area in sarcomas from mice treated with isotype control antibody (blue) or anti-Ly6G antibody (red) 48 hours after 0 Gy (filled circles) or 20 Gy (open circles) radiation. **E**) Representative images and **F**) Quantification of hypoxia (% pimonidazole⁺ area) in sarcomas from mice treated with isotype control antibody (blue) or anti-Ly6G antibody (red) 48 hours after 0 Gy (filled circles) or 20 Gy (open circles) radiation. Error bars represent mean \pm SEM. Scale bars: 25 μ m in Panel A; 50 μ m in Panel C; 100 μ m in Panel E.

Supplementary Tables

Table S1. Patient and tumor characteristics.

Patient and tumor characteristics	All patients: n=299
Median age in years (Range)	51 (18-90)
Histology	
Squamous	247 (83%)
Adenocarcinoma	46 (15%)
Adenosquamous	4 (1.3%)
Poorly-differentiated	2 (0.7%)
FIGO stage	
Ib1	35 (12%)
Ib2	89 (30%)
IIa	2 (0.7%)
IIb	101 (34%)
IIIa	4 (1.3%)
IIIb	57 (19%)
IVa	11 (4%)
Metabolic tumor volume (cc)*	27 (1-398)
Cervix SUVmax**	16 (3-60)
PET lymph nodes	
None	131 (44%)
Pelvic	118 (39%)
Pelvic + Aortic	47 (16%)
Pelvic + Aortic + Supraclavicular	3 (1%)

Supplementary Table 1. Baseline patient and tumor characteristics. * 249 patients with data; ** 278 patients with data.

Table S2. ANC association with outcomes (univariable analysis).

ANC	Cervix recurrence		Pelvic recurrence		Distant recurrence		Cancer death	
	HR (95% CI)	P value	HR (95% CI)	P value	HR (95% CI)	P value	HR (95% CI)	P value
Pre-Tx	1.05 (0.86-1.29)	0.62	1.02 (0.88-1.18)	0.83	0.995 (0.89-1.12)	0.93	1.03 (0.91-1.16)	0.63
1 wk	1.14 (1.03-1.25)	0.008	1.11 (1.02-1.22)	0.015	1.11 (1.03-1.19)	0.005	1.15 (1.07-1.23)	< 0.001
3 wk	1.18 (1.01-1.37)	0.03	1.13 (0.98-1.31)	0.08	0.97 (0.83-1.13)	0.67	1.04 (0.91-1.18)	0.57
6-8 wk	1.29 (1.09-1.53)	0.004	1.23 (1.04-1.45)	0.018	1.03 (0.84-1.27)	0.79	1.16 (0.99-1.36)	0.07
12-26 wk	1.14 (0.98-1.32)	0.09	1.17 (1.05-1.29)	0.003	1.11 (0.998-1.23)	0.05	1.29 (1.13-1.46)	< 0.001

Supplementary Table 2. Univariable Cox regression showing ANC association with local cervix recurrence, pelvic recurrence, distant recurrence, and cancer death.

Table S3. Univariable and multivariable analyses for local cervix recurrence.

	UVA HR (95% CI)	P value	MVA HR (95% CI)	P value
<u>Week 1 ANC</u>	1.14 (1.03-1.25)	0.008	1.15 (1.04-1.27)	0.006
<u>Week 1 Hgb</u>	0.90 (0.82-0.98)	0.02	NS	
<u>PET Lymph Node Status</u>				
None	Ref			
Pelvic	0.78 (0.36-1.66)	0.51	NS	
Pelvic + Para-aortic ± SCV	2.57 (1.20-5.53)	0.02		
<u>FIGO Stage</u>				
IB1-IB2	Ref			
IIA-IIB	1.59 (0.72-3.51)	0.25	NS	
IIIA-IVA	2.61 (1.18-5.74)	0.02		
Initial metabolic tumor volume	1.009 (1.005-1.014)	<0.001	NS	
Initial cervix SUVmax	1.01 (0.98-1.05)	0.57	---	

Supplementary Table 3. Cox regression univariable (UVA) and multivariable (MVA) for local cervix recurrence including hematologic and clinical factors.

Table S4. Univariable and multivariable analyses for pelvic recurrence.

	UVA HR (95% CI)	P value	MVA HR (95% CI)	P value
<u>Week 1 ANC</u>	1.11 (1.02-1.22)	0.015	1.14 (1.04-1.25)	0.005
<u>Week 1 Hgb</u>	0.91 (0.84-0.99)	0.023	NS	
<u>PET Lymph Node Status</u>				
None	Ref			
Pelvic	1.04 (0.57-1.89)	0.91	NS	
Pelvic + Para-aortic ± SCV	2.72-1.43-5.18	0.002		
<u>FIGO Stage</u>				
IB1-IB2	Ref			
IIA-IIB	1.18 (0.64-2.18)	0.59	---	
IIIA-IVA	1.74 (0.93-3.27)	0.09		
Initial metabolic tumor volume	1.006 (1.001-1.011)	0.014	NS	
Initial cervix SUVmax	1.007 (0.98-1.04)	0.63	---	

Supplementary Table 4. Cox regression univariable (UVA) and multivariable (MVA) for pelvic recurrence including hematologic and clinical factors.

Table S5. Univariable and multivariable analyses for distant recurrence

	UVA HR (95% CI)	P value	MVA HR (95% CI)	P value
<u>Week 1 ANC</u>	1.11 (1.03-1.19)	0.005	NS	
<u>Week 1 Hgb</u>	0.91 (0.86-0.97)	0.006	NS	
<u>PET Lymph Node Status</u>				
None	Ref		Ref	
Pelvic	1.62 (0.89-2.94)	0.11	1.79 (0.76-4.20)	0.18
Pelvic + Para-aortic ± SCV	6.17 (3.42-11.1)	<0.001	6.32 (2.62-15.2)	<0.001
<u>FIGO Stage</u>				
IB1-IB2	Ref		NS	
IIA-IIB	1.34 (0.74-2.43)	0.33		
IIIA-IVA	2.79 (1.59-4.93)	<0.001		
Initial metabolic tumor volume	1.007 (1.003-1.011)	0.001	1.005 (1.001-1.010)	0.017
Initial cervix SUVmax	1.004 (0.978-1.030)	0.79	---	

Supplementary Table 5. Cox regression univariable (UVA) and multivariable (MVA) for distant recurrence including hematologic and clinical factors.

Table S6. Univariable and multivariable analyses for cause-specific survival.

	UVA HR (95% CI)	P value	MVA HR (95% CI)	P value
<u>Week 1 ANC</u>	1.15 (1.07-1.23)	<0.001	1.12 (1.03-1.19)	0.007
<u>Week 1 Hgb</u>	0.89 (0.84-0.94)	<0.001	NS	
<u>PET Lymph Node Status</u>				
None	Ref		Ref	
Pelvic	1.45 (0.84-2.49)	0.18	1.87 (0.86-4.07)	0.11
Pelvic + Para-aortic ± SCV	4.02 (2.31-7.00)	<0.001	3.28 (1.42-7.57)	0.006
<u>FIGO Stage</u>				
IB1-IB2	Ref		NS	
IIA-IIB	1.26 (0.70-2.24)	0.44		
IIIA-IVA	3.35 (1.96-5.73)	<0.001		
Initial metabolic tumor volume	1.008 (1.004-1.012)	<0.001	1.007 (1.002-1.012)	0.005
Initial cervix SUVmax	1.01 (0.99-1.04)	0.23	---	

Supplementary Table 6: Cox regression univariable (UVA) and multivariable (MVA) for cervical cancer cause-specific survival including hematologic and clinical factors.

Table S7. Genetic manipulation of neutrophils

Genotype	<i>KPM:</i> <i>Kras</i> ^{FSF-G12D/+} ; <i>Trp53</i> ^{FRT/FRT} ; <i>MRP8</i> ^{Cre} ; <i>R26</i> ^{+/+}		<i>KPMT:</i> <i>Kras</i> ^{FSF-G12D/+} ; <i>Trp53</i> ^{FRT/FRT} ; <i>MRP8</i> ^{Cre} ; <i>R26</i> ^{LSL-tdTomato/+}		<i>KPMD:</i> <i>Kras</i> ^{FSF-G12D/+} ; <i>Trp53</i> ^{FRT/FRT} ; <i>MRP8</i> ^{Cre} ; <i>R26</i> ^{LSL-DTX +}	
	Tumor Cells	Neutrophils	Tumor Cells	Neutrophils	Tumor Cells	Neutrophils
No Cre; No FlpO	WT	WT	WT	WT	WT	WT
+ FlpO (Virus Delivery)	Mutant <i>Kras</i> , <i>Trp53</i> null	No change	Mutant <i>Kras</i> , <i>Trp53</i> null	No change	Mutant <i>Kras</i> , <i>Trp53</i> null	No change
+ Cre (MPR8 Driven)	No change	No change	No change	Express tdTomato; fluorescent	No change	Express diphtheria toxin; depleted

Supplementary Table 7. Genotypes for mice with genetic manipulation of neutrophils. KP^{FRT} sarcomas with wild type myeloid cells (KPM), tdTomato fluorescently-labeled myeloid cells (KPMT), or genetic depletion of myeloid cells (KPMD) using dual recombinase technology.

Table S8. Reagents used for flow cytometry

Reagent	Source	Identifier
BD CompBeads (anti-mouse/anti-rat and anti-hamster Ig and negative control compensation beads)	BD Biosciences	552843, 552845
Purified rat anti-mouse CD16/CD32 (Mouse Fc Block); Clone 2.4G2	BD Biosciences	553142
BV421 Rat Anti-Mouse CD4; Clone GK1.5	BD Biosciences	562891
APC/Cy7 anti-mouse CD8a antibody; Clone 100714	Biolegend	100714
BV786 Hamster Anti-Mouse CD3e; Clone 145-2C11	BD Biosciences	564379
Alexa-Fluor 700 Rat anti-mouse Ly6G; clone 1A8	BD Biosciences	561236
APC-eFluor 780 anti-mouse CD11b; clone M1/70	Invitrogen	47-0112-82
BV605 Rat anti-mouse CD45; clone 30-F11	BD Biosciences	563053
Zombie Aqua Dye	Biolegend	77143

Supplementary Table 8. Antibodies and reagents for flow cytometry.

References

1. Colaprico A, et al. (2016) TCGAAbiolinks: an R/Bioconductor package for integrative analysis of TCGA data. *Nucleic Acids Res* 44(8):e71.
2. Grossman RL, et al. (2016) Toward a Shared Vision for Cancer Genomic Data. *N Engl J Med* 375(12):1109–1112.
3. Thorsson V, et al. (2018) The Immune Landscape of Cancer. *Immunity* 48(4):812–830.e14.
4. Newman AM, et al. (2015) Robust enumeration of cell subsets from tissue expression profiles. *Nat Methods* 12(5):453–457.
5. Lin AJ, et al. (2018) IMRT and image-guided adapted brachytherapy for cervix cancer. *Int J Radiat Oncol Biol Phys*. doi:10.1016/j.ijrobp.2018.11.012.
6. Dupont WD, Plummer WD Jr (1990) Power and sample size calculations. A review and computer program. *Control Clin Trials* 11(2):116–128.
7. Kirsch DG, et al. (2007) A spatially and temporally restricted mouse model of soft tissue sarcoma. *Nat Med* 13(8):992–997.
8. Lee C-L, et al. (2012) Generation of primary tumors with Flp recombinase in FRT-flanked p53 mice. *Dis Model Mech* 5(3):397–402.
9. Passegué E, Wagner EF, Weissman IL (2004) JunB deficiency leads to a myeloproliferative disorder arising from hematopoietic stem cells. *Cell* 119(3):431–443.
10. Madisen L, et al. (2010) A robust and high-throughput Cre reporting and characterization system for the whole mouse brain. *Nat Neurosci* 13(1):133–140.
11. Ivanova A, et al. (2005) In vivo genetic ablation by Cre-mediated expression of diphtheria toxin fragment A. *Genesis* 43(3):129–135.
12. Newton J, et al. (2011) Commissioning a small-field biological irradiator using point, 2D, and 3D dosimetry techniques. *Med Phys* 38(12):6754–6762.
13. Butler A, Hoffman P, Smibert P, Papalexi E, Satija R (2018) Integrating single-cell transcriptomic data across different conditions, technologies, and species. *Nat Biotechnol* 36(5):411–420.
14. Sergushichev AA (2016) An algorithm for fast preranked gene set enrichment analysis using cumulative statistic calculation. *bioRxiv*:060012.
15. Fabregat A, et al. (2018) The Reactome Pathway Knowledgebase. *Nucleic Acids Res* 46(D1):D649–D655.
16. Gu Z, Eils R, Schlesner M (2016) Complex heatmaps reveal patterns and correlations in multidimensional genomic data. *Bioinformatics* 32(18):2847–2849.
17. Towns J, et al. (2014) XSEDE: Accelerating Scientific Discovery. *Computing in Science Engineering* 16(5):62–74.